Molecular docking and dynamics of Annona muricata L. megastigmanes and metabolites on enzyme markers of breast cancer and their effect on heterodimer formation

Carrillo-Landell, Felipe G.[1*]; Reyes-Martínez, Jesús A.[2]; Alvarez-Medina, Dora A.[3]; Hernández-Barrera, Alejandra[1]; Sánchez-Ramos, Sanjuana[1]

[1] Tecnológico Nacional de México/Instituto Tecnológico Superior de Irapuato, Carr. Irapuato-Silao Km 12.5, El Copal S/N, Irapuato, Guanajuato, Mexico, C.P. 36821.
[2] Universidad Autónoma de Aguascalientes, Departamento de Química, Centro de Ciencias Básicas, Avenida Universidad 940, Fraccionamiento Ciudad Universitaria, Aguascalientes, Aguascalientes, Mexico, C.P., 20131.
[3] Universidad Virtual del Estado de Guanajuato, Hermenegildo Bustos 129-A Sur, Centro, Purísima del Rincón, Guanajuato, C.P. 36400.
* Correspondence: felipe.cl@irapuato.tecnm.mx

Citation: Carrillo-Landell, F. G., Reyes-Martínez, J. A., Alvarez-Medina, D. A., Hernández-Barrera, A. & Sánchez-Ramos, S. (2023). Molecular docking and dynamics of *Annona muricata* L. megastigmanes and metabolites on enzyme markers of breast cancer and their effect on heterodimer formation. *Agro Productividad*. https://doi.org/10.32854/agrop.v16i9.2620

Academic Editors: Jorge Cadena Iñiguez and Lucero del Mar Ruiz Posadas

Received: June 29, 2023.
Accepted: September 25, 2023.
Published on-line: November 27, 2023.

Agro Productividad, 16(10). October. 2023. pp: 79-93.

ABSTRACT

Objective: To analyze the molecular docking of secondary metabolites of soursop on the enzyme markers of breast cancer.

Design/Methodology/Approach: Crystals of PARP2 and PRMT5 enzymes were obtained from RCSB-PDB. Both crystals were processed using bioinformatic tools (*e.g.*, SWISS-MODEL, UCSF-Chimera, and ScanProsite), prior to molecular docking and dynamics. The *Annona muricata* L. metabolites were obtained from Pubchem for their use in several *in silico* analysis. The Autodock algorithm was used to obtain the molecular docking. Once the most stable conformations were obtained for the ligands of each enzyme, their complexes were subjected to 10 ns of molecular dynamics using GROMACS. Meanwhile, the HPF1-PARP2 and the MEP50-PRMT5 heterodimeric interactions were carried out using the HDOCK server. Finally, the possible biotransformation reactions were studied using QSAR models.

Results: The kaempferol-3-O-rutinoside metabolite showed potential biopharmaceutical use as an inhibitor of the PARP2 enzyme. The coreximin ligand showed potential biopharmaceutical use as an inhibitor of the PRMT5 enzyme. The inhibitor impacted the PRMT5-MEP50 interaction. The QSAR models indicated that methylation, O-glucuronidation, and O-dealkylation were the most likely biotransformation reactions among the metabolites with the highest degree of inhibition.

Study Limitation/Implications: *in silico* analysis on inhibition of key proteins.

Findings/Conclusions: The kaempferol-3-O-rutinoside chemical compound showed potential as a PARP2 inhibitor. The coreximin chemical compound showed potential as a PRMT5 inhibitor. The protein-protein interaction between PRMT5 and MEP50 was impacted by the inhibitor; however, this was not the case with the PARP2 enzyme.

Keywords: soursop, proteins, inhibition.

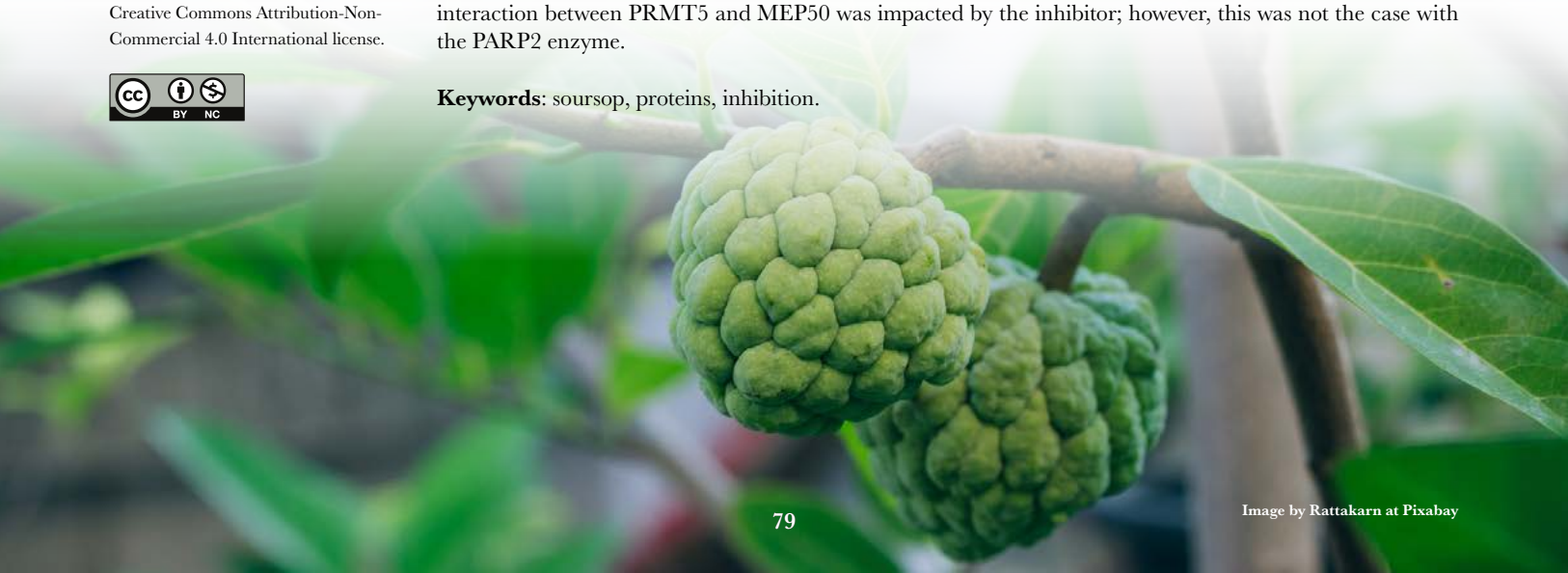

Image by Rattakarn at Pixabay

INTRODUCTION

Breast cancer is currently one of the main health problems worldwide. According to the World Health Organization (WHO) and the Pan American Health Organization (PAHO), it is the most common cause of death by cancer among women. Around a million different cases of breast cancer are detected each year and about 400,000 women die every year as a result of this disease (Ramos *et al.*, 2015). Women in countries with high socio-economic levels have a higher risk of getting breast cancer, while women in low economic levels countries face a higher risk of dying of cancer, because they cannot easily have access to healthcare services, which allows an early detection, treatment, and cure of this disease (Cárdenas *et al.*, 2015). The comprehensive treatment of breast cancer requires a multidisciplinary approach, including local-regional and systemic treatments. Surgery and radiotherapy are the chosen local-regional treatments and they include three types: neoadjuvant, adjuvant, and palliative. Meanwhile, the systemic treatment includes chemotherapy, endocrine therapy, and molecular target therapy (Arce *et al.*, 2011). Currently, the inhibition of the catalytic activity of poly (ADP-ribose), polymerase 2 (PARP2), and PRMT5 (argine protein n-methyltransferase 5) —as well as other specific enzymes that are important for survival and the behavior of cancer cells— has been suggested as an study objective (Murai *et al.*, 2012; Wang *et al.*, 2018). The PARP 2 enzyme belongs to the PARP family. These enzymes bind themselves to the damaged DNA through their zinc finger protein motif in the aminus terminal, activating their catalytic region near the carboxyl terminus and hydrolyzing the NAD+, which produces lineal and branched PAR chains. These chains can expand through hundreds of ADP-ribose units. The action produced by this enzyme in the damaged DNA plays an important role, activating the repair pathways in a single chain or breaking both DNA chains (Murai *et al.*, 2012). In response to the damage caused in the DNA, the PAR post-translational modification mainly takes place in the serine amino acids, involving the participation of the HPF1 factor, which changes the specificity of the glutamate residue left by the serine in PARP2 (Bilokapic *et al.*, 2020). Different PARP2 inhibitors (such as olaparib, veliparib, and MK-4827) are found in the advanced stage of clinical trials. The aim is to use them to treat several types of cancer (Murai *et al.*, 2012). Human beings have a total of 9 proteins of the PRMT family and they are divided into three different types. These enzymes transfer a methyl group of the S-Adenosyl methionine (SAM) to the arginine residues found in the histones, releasing an equivalent of S-Adenosyl-L-homocysteine (SAH) (Wang *et al.*, 2018). The Type II PRMTs include PRMT5 and PRMT9, which can catalyze the ω-NG-monomethylarginine (MMA) and ω-NG, NG–Symmetric dimethylarginine (sDMA) (Kim *et al.*, 2020). PRMT5 is the main enzyme in change of the symmetric dimethylation in the arginine residues of the histones, controlling and consequently regulating several biological processes that take place in the cells of mammals (Wang *et al.*, 2018). Owing to the WD repeat domain, the PRMT5 develops stable complexes, using the MEP50 factor. The *in vitro* formation of this complex favors the symmetric monomethylation and dimethylation of the histones, as a result of the high affinity that both enzymes have for the SAM substrate (Wang *et al.*, 2018; Kim *et al.*, 2020). Methylation caused by the PRMT proteins has an essential function in the development of cancer cells, including the regulatory function of PRMT5 in the gene expression involved in

tumor formation (Kim *et al.*, 2020). Two types of inhibitors can mainly inhibit the PRMT5: SAM uncompetitive inhibitors and SAM competitive inhibitors (Richters, 2017). The latter include drugs such as sinefungin, which is of natural origin and is a great inhibitor of PRMT5; however, as a result of its similarity to the SAM compound, it usually inhibits other methyltransferase proteins (Wang *et al.*, 2018). Currently, some patients have been known to develop resistance to cancer medicines, most of which have cytotoxic effects that hinder cell proliferation, regardless of the healthy or malignant characteristics of the said cells. Natural products have always been a focus of interest in the fight against cancer; some of these products include alkaloids (vinca), terpene (paclitaxel), or etoposides (Efferth *et al.*, 2017). The National Cancer Institute of Sudan has proved that 69% of the anti-cancer medicines developed from 1980 to 2002 have a natural origin (Newman *et al.*, 2007).

MATERIALS AND METHODS

Obtaining crystals and ligands

The crystals of the PARP2 and PRMT5 enzymes came from a *Homo sapiens* organism and were obtained from the RCSB PDB (Protein Data Bank) data base (https://www.rcsb.org/). The crystal with ID 4ZZX was chosen as model for PARP2, while the ID 6V0P was used for the *in silico* studies of PRMT5. In the case of the PARP2 crystals, the missing amino acids were completed in the 3D model. The task was carried out with Expasy's SWISS-MODEL (https://swissmodel.expasy.org/). Finally, the structures were visualized using the UCSF Chimera v.1.16 software, while the Expasy's ScanProsite (https://prosite.expasy.org/) was used to obtain their conserved domain. The ligands from *Annona muricata* L. used in the in silico studies were obtained from a list developed by Moghadamtousi *et al.* (2015). The focus was put on those compounds with alkaloid-type structures. Afterwards, those compounds were searched in the NCBI Pubchem data base (https://pubchem.ncbi.nlm.nih.gov/).

Ligand-Protein Molecular docking

The same structural procedure was used for both enzymes before the molecular docking. The crystals were cleaned using the Chimera v.1.16 software, adding polar hydrogens and Kollman charges with AutoDock Tools v.1.5.6. In the case of the ligands, their structure was minimized and protonated under a 7.4 pH, using the Avogadro v.1.2.0 software and a MMFF94 force field. Subsequently, the Gaisteiger charges were calculated using the AutoDock Tools v.1.5.6. The molecular docking of each enzyme and their ligands was carried out using the algorithm of the AutoDock v.4.2 software. A 68×68×68 box was developed for the PARP2 enzyme; this box contained the determining area of its catalytic action (136-363 aa). Meanwhile, a 76×76×76 box was generated for the PRMT5 enzyme, covering amino acids 308 to 463. The structure with the best docking energy of each ligand and its respective enzyme were kept as a complex. Afterwards, they were analyzed using the Protein Plus tool (https://proteins.plus/) to obtain 2D images of the ligand-protein interactions. Another molecular docking was carried out between PARP2 and the isoindolinone compound to validate the molecular dockings of PARP2, following the already mentioned parameters. Subsequently, the RMSD was calculated,

using the USCF Chimera v.1.16 software. This calculation was carried out with the best isoindolinone compound obtained from the molecular docking (PARP2-isoindolinone) and the isoindolinone from the crystal. The same validation procedure was used for PRMT5, using isoindolinone instead of sinefungin.

Molecular dynamics

A total of two molecular dynamics were carried out. The models were the best structure of the Kaempferol-3-O-rutinoside-PARP2 complex and the best structure of the Coreximin-PRMT5 complex. The GROMACS v.2022.2 software was used to develop the molecular dynamics. The conditions were the same for both models: a simulation was carried out inside a water box, adding Na+ and Cl− ions, using the Monte-Carlo method, to neutralize the charges of the complexes. The distance between the edge of the boxes and the models was 1.5 nm. The energies were minimized following the steepest descent method (615 steps), while the system was balanced at 125 ps, keeping the NVT values constant. The models obtained after the minimization and the balance were used to start the production stage. The simulation included temperature conditions of 310.15 K and a pressure of 1 bar. The whole simulation lasted 10 ns. The full process was carried out using a CHARMM36m force field. In order to determine RMSD and RMSF, the results were analyzed using the functions of the GROMACS v.2022.2 software: the formation of the hydrogen bonding between the ligand and the protein was carried out using the gmx_hbond function; the distance between the ligand and the protein was measured using the gmx_pairdist function; and the total energy of the complexes was obtained using the gmx_energy function. A structural alignment between the models was performed, using the MatchMaker tool of the UCSF Chimera v.1.16 software. This process was used to analyze the structural differences between the PARP2 (PDB) and PARP2-kaempferol-3-O-rutinoside models and the PRMT5 (PDB) and PRMT5-coreximin models, after the molecular dynamics were carried out. Additionally, the four models were analyzed using the PROCHECK tool to obtain the Ramachandran plots and to compare the amino acid torsion.

Protein-protein molecular docking

Given the importance of the HPF1-PARP2 and MEP50-PRMT5 complexes formation for the appropriate functioning of these enzymes (Suskiewicz *et al.*, 2020; Antonysamy, 2017), the potential differences of the interactions between the HPF1-PARP2 and HPF1-PARP2-kaempferol-3-O-rutinoside and the MEP50-PRMT5 and MEP50-PRMT5-coreximin were analyzed. The PARP2 and PRMT5 models obtained from the molecular dynamic were used for this purpose. Additionally, the PARP2 and PRMT5 crystals were used to carry out the dockings with HPF1 and MEP50, respectively. The crystal of the human HPF1 (ID 6M3G) was obtained from the RCSB PDB (Protein Data Bank) data base. The missing amino acids were added to the crystal, after they had been reconstructed by homology using Expasy's SWISS-MODEL. The MEP50 structure (ID 7U30) was also obtained from the same data base (Table 1). All the dockings between proteins were carried out using the HDOCK online server (http://hdock.phys.hust.edu.cn/). The result

of the HPF1-PARP2-kaempferol-3-O-rutinoside docking was compared with the crystal of the 6TX3 complex (obtained from the same data base); meanwhile, the MEP50-PRMT5-coreximin docking was compared with the 7U30 crystal. Both comparisons were carried out using the UCSF Chimera v.1.16 software.

In silico analysis of the biotransformation

A study of the potential biotransformations of the kaempferol-3-O-rutinoside, coreximin, and coclaurine compounds inside the human body was carried out. These changes could have an impact on the ability of the compound to inhibit the target enzyme. The Way2Drug (http://www.way2drug.com/) online tools were used to carry out this analysis. The potential chemical reactions within the human body and the potential metabolic area were determined using the Reactive Atom tool. The PASS and SOMP tools were used to establish which enzymes could generate first and second phase metabolism in the compounds.

RESULTS AND DISCUSSION

Obtaining the crystals and ligands

The human PARP2 crystal used during the experiment was 363-amino acids long; it had a molecular weight of 82.70 kDa for the complex and a 1.65 Å resolution. It was obtained using the x-ray diffraction technique, with overall good quality metrics. Two domains were found between the amino acids 11 to 128 (PARP alpha helical domain) and 136 to 363 (catalytic domain). For its part, the human PRMT5 crystal was 637-amino acids long; it had a molecular weight of 110.48 kDa for the complex and a 1.88 Å resolution. It was also obtained from an x-ray diffraction, with overall good metrics (Table 1): Its domain was found between residues 308 to 615 (PRMT type domain, SAM-dependent methyltransferase). A total of 21 ligands were tested, 18 of which were evaluated in both enzymes (Table 2). Ten of the 18 ligands were megastigmanes, while 8 were alkaline.

Ligand-Protein molecular docking

In the case of PARP2, the best compound was Kaempferol-3-O-rutinoside, given its high binding capacity (−11.46 kcal/mol binding energy). This compound derived from megastigmanes. Regarding PRMT5, the alkaloid coreximin compound recorded the best binding capacity (−10.33 kcal/−mol binding energy). The coclarine compound had

Table 1. Crystals of the enzymes used during the research (obtained from the RCSB PDB).

Crystal (PDB ID)	No. Amino acids	Crystal molecular weight (kD)	Resolution (Å)	Technique
PARP2 (4ZZX)	363	82.70	1.65	X-ray diffraction
PRMT5 (6V0P)	637	110.48	1.88	X-ray diffraction
HPF1 (6M3G)	356	39.50	1.57	X-ray diffraction
HPF1-PARP2* (6TX3)	598	68.97	2.96	X-ray diffraction
MEP50-PRMT5 (7U30)	325	109.46	2.60	X-ray diffraction

*Catalytic fragment of the PARP2 protein.

the best binding capacity for both enzymes, obtaining a −9.48 kcal/mol and −9.79 kcal/mol binding union for PARP2 and PRMT5, respectively. This compound is an alkaloid (Table 3).

Table 2. Ligands used for the molecular docking of the PARP2 and PRMT5.

Ligand	Pubchem ID	Type	Enzyme used	Binding energy (kcal/mol)
Annoionol A	101564134	Megastigmane	PARP2 PRMT5	−7.03 −7.20
Annoionol B	101564135	Megastigmane	PARP2 PRMT5	−6.83 −6.55
Annoionoside	101564136	Megastigmane	PARP2 PRMT5	−7.01 −7.59
Roseoside	9930064	Megastigmane	PARP2 PRMT5	−8.13 −6.57
Citroside A	14312560	Megastigmane	PARP2 PRMT5	−9.18 −5.81
Blumenol C	118284	Megastigmane	PARP2 PRMT5	−7.55 −6.98
Rutin	5280805	Megastigmane	PARP2 PRMT5	−10.47 −3.87
Kaempferol-3-O-rutinoside	5318767	Megastigmane	PARP2 PRMT5	−11.46 −4.33
Kaempferol-3-O-robinobioside	15944778	Megastigmane	PARP2 PRMT5	−10.69 −5.56
Kaempferol-3-O-glucoside	10095180	Megastigmane	PARP2 PRMT5	−8.92 −9.71
Annomuricine A	157682	Alkaloid	PARP2 PRMT5	−5.99 −0.14
Reticuline	439653	Alkaloid	PARP2 PRMT5	−8.72 −9.76
Coclaurine	160487	Alkaloid	PARP2 PRMT5	−9.48 −9.79
Olaparib*	23725625	Drug	PARP2	−11.75
Coreximine	7037179	Alkaloid	PARP2 PRMT5	−8.27 −10.33
Atherosperminine	96918	Alkaloid	PARP2 PRMT5	−8.83 −9.67
Stepharine	98455	Alkaloid	PARP2 PRMT5	−8.67 −9.51
Anomurine	157218	Alkaloid	PARP2 PRMT5	−9.75 −9.45
Annomuricine	157209	Alkaloid	PARP2 PRMT5	−8.62 −9.17
Sinefungin**	65482	Nucleoside	PRMT5	−10.16

*Compound used as inhibitor of the PARP2 (commercial use).
**Compound used as inhibitor of the PRMT5 (experimental use).

Table 3. Results of the best molecular dockings for each enzyme, individually and together.

Ligand	Enzyme	Binding energy (kcal/mol)	Inhibition constant (nM)	Reference RMSD	Atoms in hydrogen bond	Amino acids
Kaempferol-3-O-rutinoside	PARP2	−11.46	4.01	58.47	5	GLY209, SER210, SER250.
Coclaurine	PARP2	−9.48	111.48	57.44	4	GLY209, ASN214, GLN112, SER250.
Olaparib*	PARP2	−11.75	2.46	59.04	3	TYR242, GLY209.
Coclaurine	PRMT5	−9.79	66.54	100.8	3	MET420, GLU392, GLU444.
Coreximine	PRMT5	−10.33	26.87	95.86	1	LEU437.
Sinefungin**	PRMT5	−10.16	35.62	99.66	5	LYS333, LEU437, GLU392, GLU444.

***Compound used as inhibitor of the PARP2 (commercial use).
****Compound used as inhibitor of the PRMT5 (experimental use).

The interactions between the Kaempferol-3-O-rutinoside-PARP2 compound obtained with Protein Plus show a hydrogen bonding formation with the Ser250, Gly209, Glu338, Ser210, Glu115, and Arg224 residues, while hydrophobic interactions were recorded with the Tyr253, His208, and Tyr242 amino acids (Figure 1A). Meanwhile, the hydrophobic interactions of the coreximin-PRMT5 complex took place with the Glu435, Phe327, Pro314, and Leu436 amino acids, while the hydrogen bonding formation took place with the Glu444, Cys449, Leu437, and Lys333 amino acids (Figure 1B). For its part, the coclaurine-PARP2 complex had hydrophobic interactions with the Tyr253 and Ser210 residues and hydrogen bonding formations with Ser250, Gly209, Gln112, and Asn214 amino acids (Figure 1C). In the case of the coclaurine-PRMT5 interactions, the hydrogen bonding formation took place with the Met420, Glu392, Tyr324, and Glu444 residues, while hydrophobic interactions were observed with the Pro314, Gly365, and Lys393 amino acids (Figure 1D). The RMSD between the best isoindolinone formation —resulting from the second molecular docking— and the isoindolinone in the PARP2 crystal —used for the in silico trials— recorded a result of 5.573 Å. Regarding the PRMT5, the RMSD between the best formation of the sinefungin obtained after the second molecular docking and the sinefugin in the crystal was 6.652 Å, which validates de molecular dockings carried out with both enzymes.

Molecular dynamics

The results of the molecular dynamic for the PARP2 complex and its ligand showed an acceptable stability between PARP2 and the kaempferol-3-O-rutinoside. The RMSD value was <3 Å, while the RMSD of the protein and the ligand did not exceed 2 Å and 1 Å, respectively. These values were constant during the 10ns that the simulation lasted (Figure 2A). The RMSF graph for the complex shows low energy levels for most of the amino acids with which the kaempferol-3-O-rutinoside interacts, which favors the bonding and the stability of the compound and the enzyme. However, some of the enzyme's zones are not favorable to this interaction, such as the >300-residues area (Figure

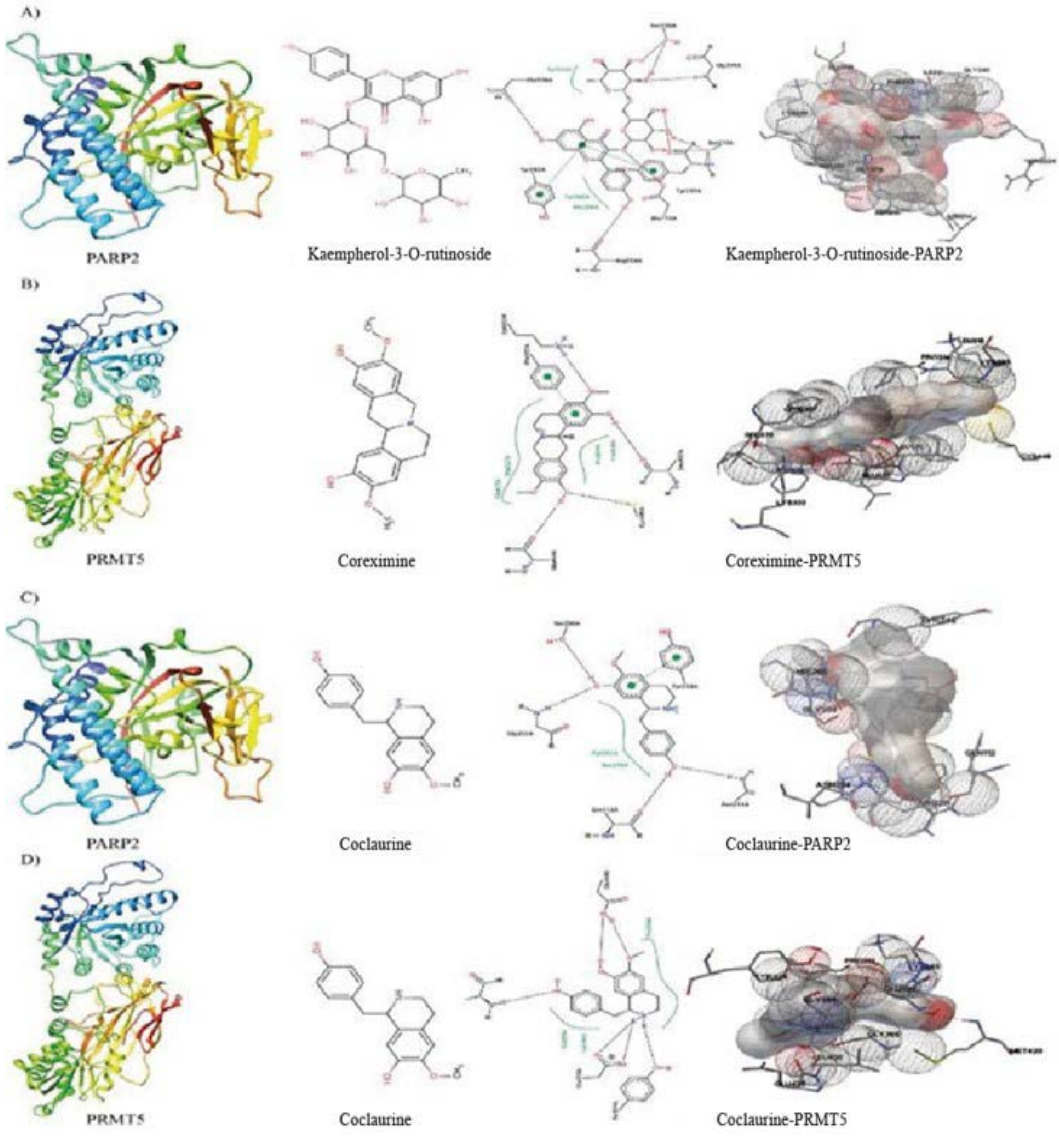

Figure 1. Best results obtained from the molecular docking between the soursop metabolites and the PARP2 and PRMT5 enzymes. The interactions between the molecules are shown as 2D diagrams (ProteinPlus; center) and 3D (Autodock Tools; right). A) Molecular docking between PARP2 and kaempferol-3-O-rutinoside; B) molecular docking between PRMT5 and coreximine; C) molecular docking between PARP2 and coclaurine; and D) molecular docking between PRMT5 and coclaurine.

2B). Regarding the formation of hydrogen bondings (HB) between the kaempferol-3-O-rutinoside and the PARP2, the simulation showed that, during the 10 ns of the dynamic, the maximum number of HB was 10 —a figure recorded before the simulation reached 2 ns. The minimum HB was reached before 1ns. However, a good number of HB links were recorded in the complex throughout the simulation (Figure 2C). The distance between the PARP2 residues and their ligand varied constantly during the whole 10 ns, with a minimum and maximum distances of 0.155 nm and 0.2 nm, respectively (Figure 2D). After the dynamics, the total energy of the system reached approximately −3.8e+05 KJ/mol

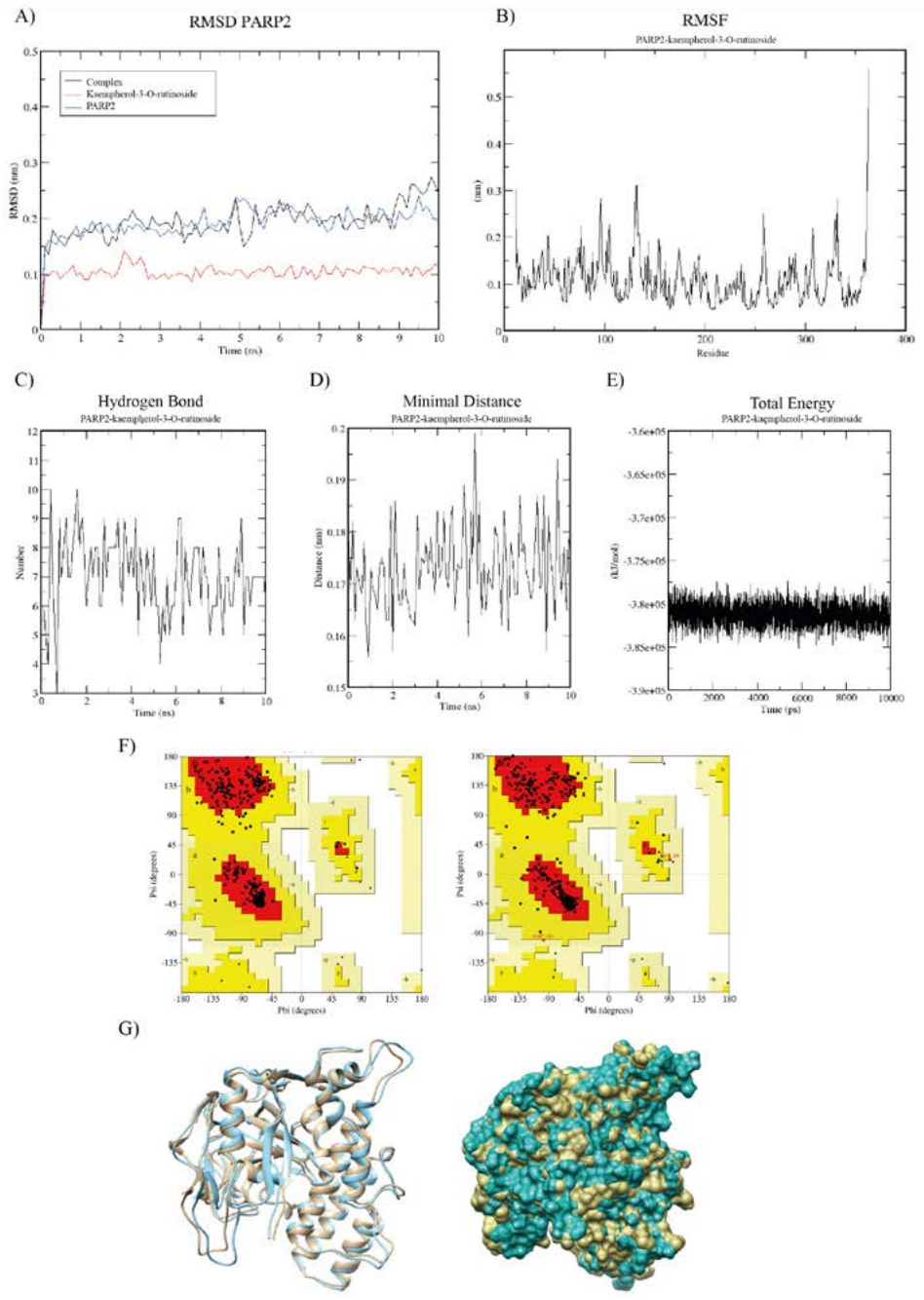

Figure 2. Results obtained after 10 ns of molecular dynamics, using GROMACS for the PARP2 and kaempferol-3-O-rutinoside complex. A) Quadratic median deviation in the structure of the PARP2, of the kaempferol-3-O-rutinoside, and of the complex resulting from both; B) quadratic median deviation of the total energy flows resulting from the PARP2 and kaempferol-3-O-rutinoside complex; C) formation of the hydrogen bondings between the ligand and the enzyme, developed during the 10 ns of molecular simulation; D) variation of the distance between the ligand and the enzyme during the 10 ns of the simulation; E) total energy of the system during the whole simulation, after the minimization, the balance, and the production; F) Ramachandran plots before the detection of kaempferol-3-O-rutinoside (left) and after the detection, during the molecular dynamic (right); G) structural changes caused by kaempferol-3-O-rutinoside (cream) and the PARP2, after the detection of kaempferol-3-O-rutinoside (blue); G) treadmill model (left) and sphere model (right) of the overlay proteins.

(Figure 2E). The structural comparison between the PARP2-kaempferol-3-O-rutinoside and the PARP2 crystal showed a clear torsion of the angles of the residues; the change was more significant for the Lys39 and ASP330 amino acids (Figure 2F). Overall, this change in the angles of the protein modified some hydrophobic areas, therefore altering the surface of the protein (Figure 2G). The PRMT5- coreximin and the protein by itself kept a <3 Å total RMSD value, throughout the 10 ns of the simulation, while the RMSD value for the coreximin was <1 Å during the whole simulation (Figure 3A). The RMSF analysis showed an unstable binding between the 150 and 200 residues of the PRMT5, while the residues where the ligand-protein interaction is more likely to take place are found between amino acids 300 and 500 (Figure 3B). The distance between the coreximin and the PRMT5 ranged between 0.17 nm and 0.19 nm during the 10 ns of the simulation, reaching a minimum and maximum distances of 0.155 nm and >0.21 nm, respectively (Figure 3C).

The formation of hydrogen bondings between the PRMT5 and the coreximin resulted in a 1-2 variant, during most of the simulation (Figure 3D). The total energy of the system during the 10 ns of the simulation remained close to −1.483+06 KJ/mol (Figure 3E). The comparison between the structures of the PRMT5-coreximin model and the crystal of the PRMT5 showed small changes in the rotation of some amino acids and in the surface of the protein (Figures 3F and 3G).

The molecular docking between HPF1 and PARP2-kaempferol-3-O-rutinoside (recorded after the molecular dynamic) was carried out in the HDOCK server and recorded a −423.79 docking score and a 0.69 RMSD ligand. Meanwhile, the HPF1 and PARP2 complex (obtained from the PDB) had a 0.40 RMSD and a −363.73 docking score. The analysis of the docking between the PARP2-kaempferol-3-O-rutinoside, the PARP2 (obtained from the PDB), and the HPF1 (obtained with UCSF Chimera v.1.16) showed that the His381 residue of the PARP2-kaempferol-3-O-rutinoside moved away from the ASP283 residue of the HPF1, increasing from 2.10 Å to 2.78 Å (Figure 4A and Table 4). In the case of the docking between the MEP50 and the PRMT5-coreximin, the PRMT5 lost its binding capacity with the MEP50 in the expected area, while the ARG63 and ARG67 of the PRMT5 did not interact with the Trp44 and Phe289 amino acids of the MEP50. In this case, the docking score was −236.47, while the RMDS was 174.40. Finally, the docking between MEP50 and PRMT5 (obtained from PDB) kept the interaction between the said amino acids, reaching a docking score of −678.96 and a RMSD of 71.16 (Figure 4B and Table 4).

Biotransformation *in silico* analysis

The potential reactions to the kaempferol-3-O-rutinoside compound within a human body include: methylation, O-glucuronidation, hydrolysis, and O-sulfation; the most common reactions are methylation (76.3%) and O-glucuronidation (61.3%). Regarding coreximin, the potential reactions include O-glucuronidation, O-dealkylation, O-sulfation, methylation, and aliphatic hydroxylation; the results indicate that the most common reactions are O-glucuronidation (55.8%) and O-dealkylation (50.2%).

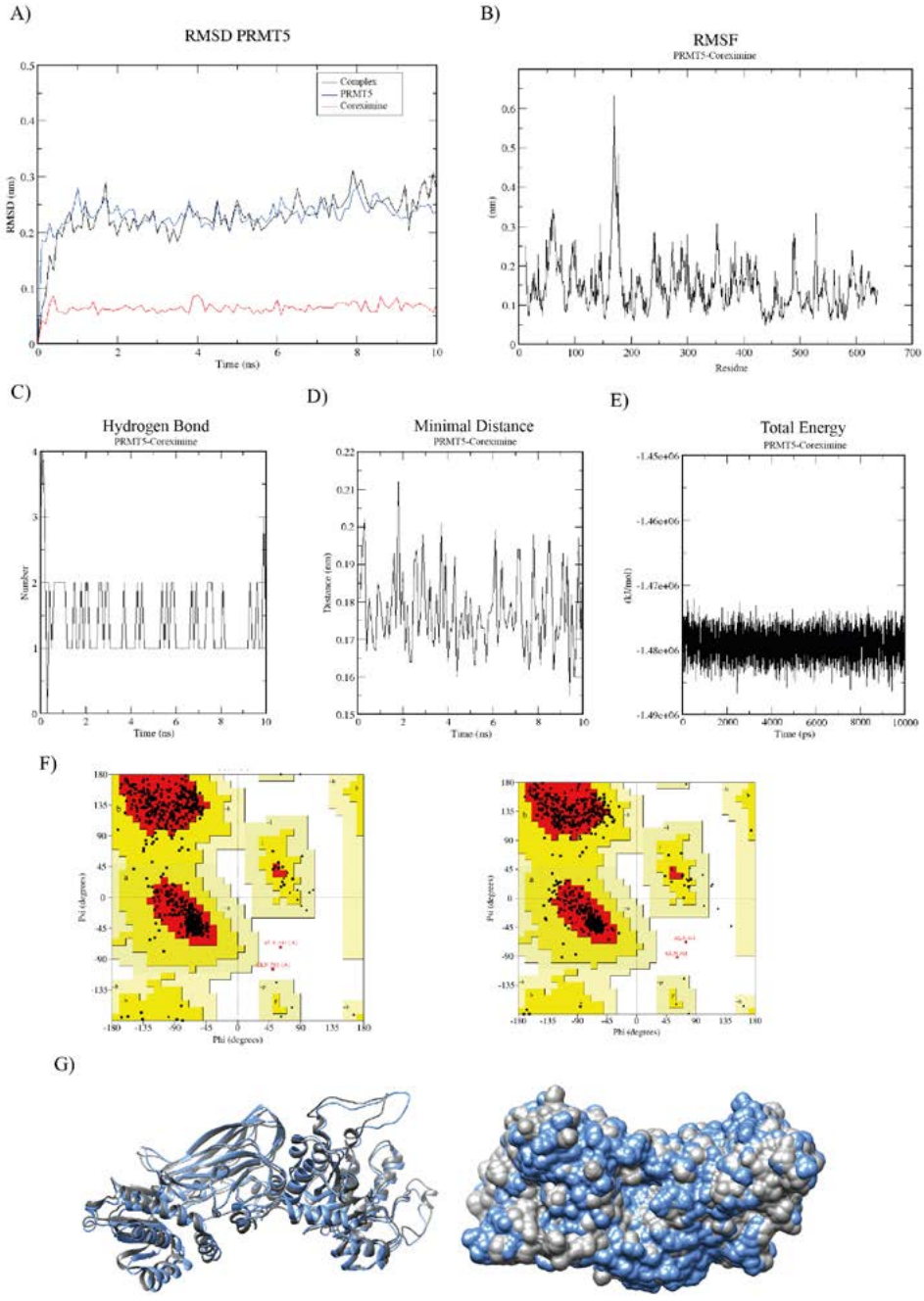

Figure 3. Results obtained after 10 ns of molecular dynamics, using GROMACS for the PRMT5 and coclaurine complex. A) Quadratic median deviation in the structure of the PRMT5, of the coclaurine, and of the complex resulting from both; B) quadratic median deviation of the total energy flows resulting from the PRMT5 and coclaurine complex; C) formation of the hydrogen bondings between the ligand and the enzyme, developed during the 10 ns of molecular simulation; D) variation of the distance between the ligand and the enzyme, during the 10 ns of the simulation; E) total energy of the system during the whole simulation, after the minimization, the balance, and the production; F) Ramachandran plots before the detection of coclaurine (left) and after the detection, during the molecular dynamics (right); G) structural changes caused after the molecular dynamics and the detection of the ligand, the PRMT5 before the presence of the coclaurine (gray) and the PRMT5 after the presence of the coclaurine (blue). G) treadmill model (left) and sphere model (right) of the overlay proteins.

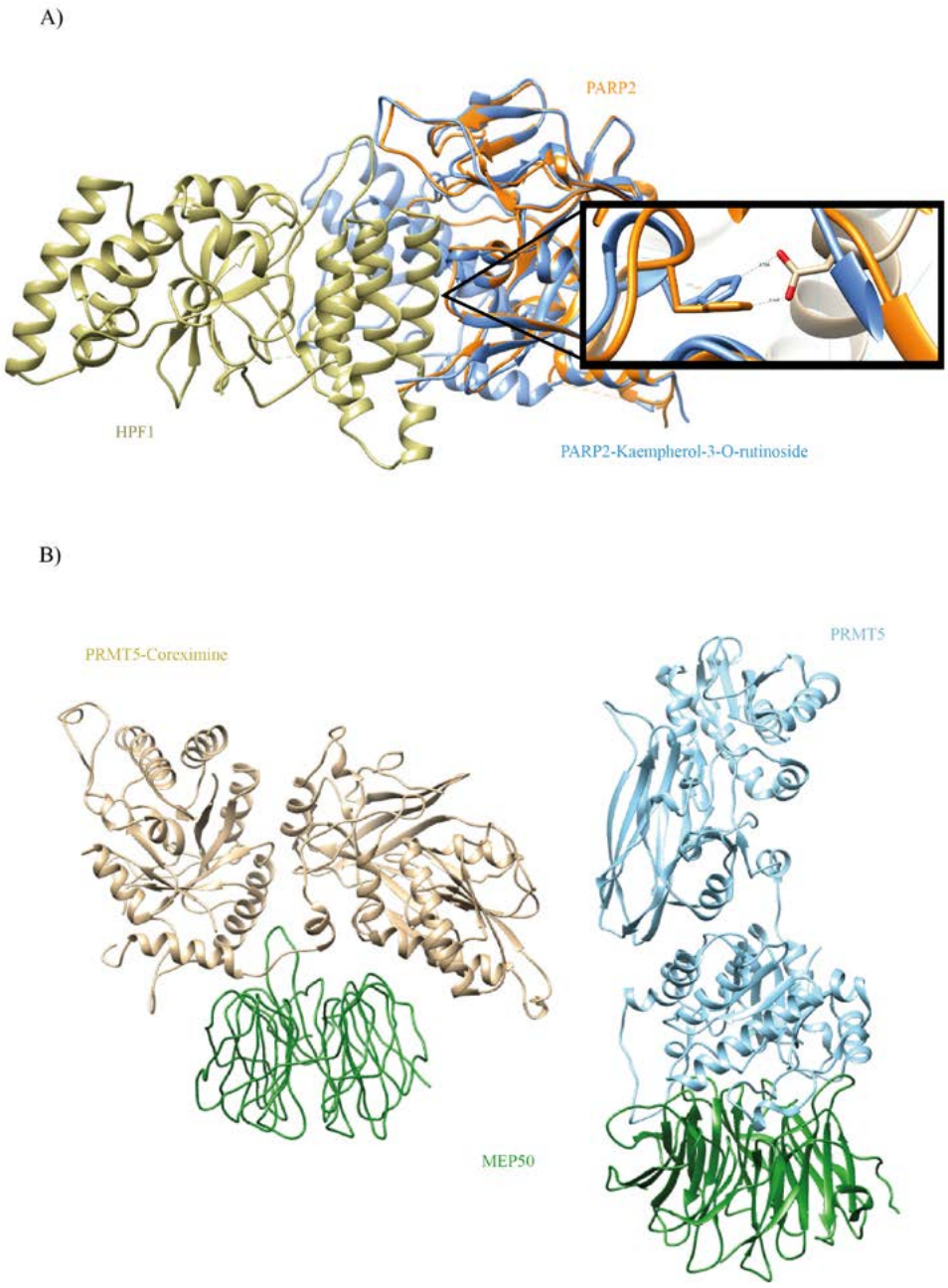

Figure 4. Comparison between the HPF1 and PARP2 interactions. Golden: HPF1; orange: PARP2 without the changes produced by the kaempferol-3-O-rutinoside; blue: PARP2 with the structural changes caused by the molecular dynamics in the presence of the kaempferol-3-O-rutinoside. A) A 0.68 Å change in the distance between the His381 residue of the PARP2 and the Asp283 of the HPF1; B) comparison between the MEP50 and PRMT5 interactions. Green: MEP50; blue: PRMT5 without coreximin; brown: PRMT5 with the structural changes caused by the molecular dynamics in the presence of the coreximin. Coreximin had a significant impact on the MEP50 and PRMT5 interactions.

Meanwhile, the reactions caused by coclaurine included O-dealkylation, O-sulfation, O-glucuronidation, and methylation; the most common reaction was O-dealkylation (60.8%) (Table 5).

Table 4. Predicted reactions for the reactive atom tool of Way2Drug. ΔP value (Activity probability [AP] - Inactivity probability [IP]) shows the probability that the said reaction takes place.

Compound	SMILES of the compound	W2D/RA (ΔP)
Kaempferol-3-O-rutinoside	CC1C(C(C(C(O1)OCC2C(C(C(C(O2)OC3=C(OC4=CC(=CC(=C4C3=O)O)O)C5=CC=C(C=C5)O)O)O)O)O)O)O	Methylation (0.763) O-Glucuronidation (0.613) Hydrolysis (0.186) O-Sulfation (0.220)
Coreximine	COC1=C(C=C2C3CC4=CC(=C(C=C4C-N3CCC2=C1)OC)O)O	O-Glucuronidation (0.558) O-Dealkylation (0.502) O-Sulfation (0.453) Methylation (0.420) Aliphatic hydroxylation (0.279) Aromatic hydroxylation (0.228) Dehydrogenation (0.154) N-Glucuronidation (0.039)
Coclaurine	COC1=C(C=C2C(NCCC2=C1)CC3=CC=C(C=C3)O)O	O-Dealkylation (0.608) O-Sulfation (0.288) O-Glucuronidation (0.246) Methylation (0.231)

The PASS and SOMP results showed that the enzymes that might cause deteriorations to the kaempferol-3-O-rutinoside, through first phase metabolic reactions, are the CYP3A4 (50.3%), CYP2C9 (28.3%), and CYP1A2 (36.9%) cytochromes. Meanwhile, the O-glucuronaidation (which belongs to the second phase metabolism) could be caused by the UDP-Glucuronyl Transferase (UGT) enzyme (94.8%). In the case of coreximin, the first phase metabolism would be caused by the CYP3A4 (34.8%), CYP2D6 (56.5%), CYP2C19 (39.4%), CYP2C9 (3%), and CYP1A2 (11.8%) cytochromes. The UGT has a low involvement in the second phase metabolism (19.4%). The CYP2D6 (16.7%) cytochrome is the only cytochrome involved in the first phase metabolism of coclaurine. It has a low affinity with the UGT enzyme, during the second phase metabolism (28%) (Table 6).

Molecular docking is currently one of the most effective and used methods for the *in silico* analysis of the potential interactions between molecules and their biological objectives. This process is usually focused in the prediction of the formation of the ligand based on the receptor molecule. Its affinity is subsequently estimated using a scoring function. These tools enable the understanding of how the chemical compounds interact with their molecular objective, leading to the development of innovative drugs (Pinzi *et al.*, 2019).

Table 5. Probability that the Kaempferol-3-O-rutinoside, coreximin and coclaurine compounds become substrates of the CYP (first phase metabolism) and UGT (second phase metabolism) isoforms. The recorded values are the ΔP (PA-Pi), obtained from the PASS and SOMP tools, both in the Way2Drug server.

	First phase metabolism					Second phase metabolism
Compound	**CYP3A4**	**CYP2D6**	**CYP2C19**	**CYP2C9**	**CYP1A2**	**UDP-Glucuronyl Transferase**
Kaempferol-3-O-rutinoside	0.503	-	-	0.283	0.369	0.948
Coreximine	0.348	0.565	0.394	0.030	0.118	0.194
Coclaurine	-	0.167	-	-	-	0.280

Table 6. Results of the protein-protein docking obtained in the HDOCK server.

Model	Docking score	RMSD Ligand
HPF1-PARP2-Kaempferol-3-O-rutinoside	−423.79	0.69
HPF1-PARP2 (PDB)	−363.73	0.40
MEP50-PRMT5-Coreximine	−236.47	174.40
MEP50-PRMT5 (PDB)	−678.96	71.16

In addition to the molecular docking, tools such as simulations or molecular dynamics are very important for the accurate prediction of the molecule-receptor interaction. This process has drastically expanded during the last few years (Pinzi *et al.*, 2019; Hollingsworth and Dror, 2018).

The molecular docking between the PARP2 protein and the kaempferol-3-O-rutinoside compound has a similar binding capacity to the one shown by olaparib, a residue used to bind the substrate of the PARP2. The presence of kaempferol-3-O-rutinoside in PARP2 caused changes in the rotation of the amino acids of the protein; however, they did not affect the formation of the HPF1-PARP2 heterodimer. Likewise, the binding capacity of the molecular docking between the PRMT5 enzyme and the coreximin compound was very similar to the one shown by sinefungin. This compound is used as inhibitor of the PRMT5. Just like in the case of PARP2, the PRMT5-coreximin complex shows stability after a 10-ns long simulation. Therefore, coreximin has the potential to be used as an inhibitor of the PRMT5. The presence of coreximin in the PRMT5 gave rise to structural changes in the protein, causing an important impact on the MEP50-PRMT5 interaction.

The Quantitative Structure Activity Relationship (QSAR) models are computational methods based on mathematical models, used to search for statistically important relationships between the structures and the functioning of chemical compounds. They are currently used as a major prediction tool during the creation of innovative medicines (Verma *et al.* 2010). Applying these tools to the kaempferol-3-O-rutinoside, coreximin, and coclaurine compounds showed that they are susceptible to such reactions as methylation, O-glucuronidation, and O-dealkylation. These reactions can be caused by the UDP-Glucuronyl Transferase enzymes or by the CYP3A4, CYP2D6, CYP2C19, CYP2C9, and CYP1A2 cytochromes. These first and second phase metabolisms are not uncommon, because they are some of the most common reactions that take place when drugs are introduced into the human body.

CONCLUSIONS

The kaempferol-3-O-rutinoside compound has the potential to become an inhibitor of the PARP2 enzyme; however, according to the QSAR models, it undergoes methylation and O-glucuronidation within the human body. The presence of this compound had no impact on the HPF1-PARP2 heterodimer formation. The coreximin compound showed the potential to become an inhibitor of the PRMT5 enzyme; however, according to the QSAR model, it experiences O-dealkylation and O-glucuronization within the human body. The presence of this compound did not have an impact on the formation of the

MEP50-PRMT5 heterodimer. Performing in vitro experiments might corroborate the inhibitory capacity of these soursop compounds on growth-relevant enzymes and in the development of cancer cells.

REFERENCES

Antonysamy S. (2017). The Structure and Function of the PRMT5:MEP50 Complex Sub-cellular biochemistry, 83, 185–194.

Arce, C., Bargalló, E., Villaseñor, Y., Gamboa, C., Lara, F., Pérez, V., & Villarreal, P. (2011). Cáncer de mama. Instituto Nacional de Cancerología.

Avogadro Chemistry. (2016). Avogadro. Retrieved from http://avogadro.cc/.

Bilokapic, S., Suskiewicz, M. J., Ahel, I., & Halic, M. (2020). Bridging of DNA breaks activates PARP2-HPF1 to modify chromatin. *Nature, 585*(7826), 609–613.

Cárdenas-Sánchez, J., Bargalló-Rocha, E., Erazo-Valle, A., Chacón, A. P., Valero-Casti- llo, V., & Pérez-Sánchez, V. (2015). Consenso Mexicano sobre diagnóstico y tratamiento del cáncer mamario. *Gaceta Mexicana de Oncología, 14*(Supl 2), 2-55.

De Castro E, Sigrist CJA, Gattiker A, Bulliard V, Langendijk-Genevaux PS, Gasteiger E, Bairoch A, Hulo N. ScanProsite: detection of PROSITE signature matches and ProRule-associated functional and structural residues in proteins. *Nucleic Acids Res.* 2006 Jul 1;34(Web Server issue):W362-5.

Efferth, T., Saeed, M., Mirghani, E., Alim, A., Yassin, Z., Saeed, E., Khalid, H. E., & Daak, S. (2017). Integration of phytochemicals and phytotherapy into cancer precision medicine. *Oncotarget, 8*(30), 50284–50304.

Filimonov D.A., Lagunin A.A., Gloriozova T.A., Rudik A.V., Druzhilovskii D.S., Pogodin P.V., Poroikov V.V. (2014). Prediction of the biological activity spectra of organic compounds using the PASS online web resource. *Chemistry of Heterocyclic Compounds, 50*(3), 444-457.

Hollingsworth, S. A., & Dror, R. O. (2018). Molecular Dynamics Simulation for All. *Neuron, 99*(6), 1129–1143.

Huang, C.C., Couch, G.S., Pettersen, E.F., and Ferrin, T.E. "Chimera: An Extensible Molecular Modeling Application Constructed Using Standard Components." Pacific Symposium on Biocomputing 1:724 (1996).

Kim, H., & Ronai, Z. A. (2020). PRMT5 function and targeting in cancer. *Cell stress, 4*(8), 199–215.

Laskowski R A, MacArthur M W, Moss D S, Thornton J M (1993). PROCHECK - a program to check the stereochemical quality of protein structures. *J. App. Cryst.*, 26, 283-291.

McKinney, D. C., McMillan, B. J., Ranaghan, M. J., Moroco, J. A., Brousseau, M., Mullin-Bernstein, Z., O'Keefe, M., McCarren, P., Mesleh, M. F., Mulvaney, K. M., Robinson, F., Singh, R., Bajrami, B., Wagner, F. F., Hilgraf, R., Drysdale, M. J., Campbell, A. J., Skepner, A., Timm, D. E., Porter, D., … Ianari, A. (2021). Discovery of a First-in-Class Inhibitor of the PRMT5-Substrate Adaptor Interaction. *Journal of medicinal chemistry, 64*(15), 11148–11168.

Moghadamtousi, S. Z., Fadaeinasab, M., Nikzad, S., Mohan, G., Ali, H. M., & Kadir, H. A. (2015). *Annona muricata* (Annonaceae): A Review of Its Traditional Uses, Isolated Acetogenins and Biological Activities. *International journal of molecular sciences, 16*(7), 15625–15658.

Morris, G. M., Huey, R., Lindstrom, W., Sanner, M. F., Belew, R. K., Goodsell, D. S., & Olson, A. J. (2009). AutoDock4 and AutoDockTools4: Automated docking with selective receptor flexibility. *Journal of Computational Chemistry, 30*(16), 2785–2791.

Murai, J., Huang, S. Y., Das, B. B., Renaud, A., Zhang, Y., Doroshow, J. H., Ji, J., Takeda, S., & Pommier, Y. (2012). Trapping of PARP1 and PARP2 by Clinical PARP Inhibitors. *Cancer research, 72*(21), 5588–5599.

Newman, D. J., & Cragg, G. M. (2007). Natural products as sources of new drugs over the last 25 years. *Journal of natural products, 70*(3), 461–477.

Papeo, G., Posteri, H., Borghi, D., Busel, A. A., Caprera, F., Casale, E., Ciomei, M., Cirla, A., Corti, E., D'Anello, M., Fasolini, M., Forte, B., Galvani, A., Isacchi, A., Khvat, A., Krasavin, M. Y., Lupi, R., Orsini, P., Perego, R., Pesenti, E., … Montagnoli, A. (2015). Discovery of 2-[1-(4,4-Difluorocyclohexyl) piperidin-4-yl]-6-fluoro-3-oxo-2,3-dihydro-1H-isoindole-4-carboxamide (NMS-P118): A Potent, Orally Available, and Highly Selective PARP-1 Inhibitor for Cancer Therapy. *Journal of medicinal chemistry, 58*(17), 6875–6898.

Paul Bauer, Berk Hess, & Erik Lindahl. (2022). GROMACS 2022.2 Manual (2022.2). Zenodo.

Pinzi, L., & Rastelli, G. (2019). Molecular Docking: Shifting Paradigms in Drug Discovery. *International journal of molecular sciences, 20*(18), 4331.

Ramos Águila, Yisel de la Caridad, Marimón Torres, Eugenia Rita, Crespo González, Caridad, Junco Sena, Bárbara, & Valiente Morejón, Wilfredo. (2015). Cáncer de mama, su caracterización epidemiológica. *Revista de Ciencias Médicas de Pinar del Río, 19*(4), 619-629.

Richters A. (2017). Targeting protein arginine methyltransferase 5 in disease. *Future medicinal chemistry, 9*(17), 2081–2098.

Rudik A., Dmitriev A., Lagunin A., Filimonov D., Poroikov V. (2015). SOMP: web-service for in silico prediction of sites of metabolism for drug-like compounds. *Bioinformatics, 31* (12), 2046-2048.

Schöning-Stierand, K.; Diedrich, K.; Fährrolfes, R.; Flachsenberg, F.; Meyder, A.; Nittinger, E.; Steinegger, R.; Rarey, M. (2020). ProteinsPlus: interactive analysis of protein–ligand binding interfaces. *Nucleic Acids Research*, 48:W48-W53.

Suskiewicz, M. J., Zobel, F., Ogden, T., Fontana, P., Ariza, A., Yang, J. C., Zhu, K., Bracken, L., Hawthorne, W. J., Ahel, D., Neuhaus, D., & Ahel, I. (2020). HPF1 completes the PARP active site for DNA damage-induced ADP-ribosylation. *Nature, 579*(7800), 598–602.

Verma, J., Khedkar, V., & Coutinho, E. (2010). 3D-QSAR in Drug Design - A Review. *Current Topics in Medicinal Chemistry, 10*(1), 95–115.

Wang, Y., Hu, W., & Yuan, Y. (2018). Protein Arginine Methyltransferase 5 (PRMT5) as an Anticancer Target and Its Inhibitor Discovery. *Journal of medicinal chemistry, 61*(21), 9429–9441.

Waterhouse, A., Bertoni, M., Bienert, S., Studer, G., Tauriello, G., Gumienny, R., Heer, F.T., de Beer, T.A.P., Rempfer, C., Bordoli, L., Lepore, R., Schwede, T. SWISS-MODEL: homology modelling of protein structures and complexes. *Nucleic Acids Res.* 46, W296-W303 (2018).

Yan Y, Tao H, He J, Huang S-Y.* The HDOCK server for integrated protein-protein docking. *Nature Protocols*, 2020.